CHEMISTRY OF MATERIALS

pubs.acs.org/cm

Article

Ferrite Materials Containing Kagomé Layers: Chemistry of $Ba_2Fe_{11}Ge_2O_{22}$ and $K_2Co_4V_9O_{22}$ Hexaferrites

Megan M. Smart, Tiffany M. Smith Pellizzeri, Gregory Morrison, Colin D. McMillen, Hans-Conrad zur Loye, and Joseph W. Kolis*

Cite This: *Chem. Mater.* 2021, 33, 2258–2266

Read Online

ACCESS | Metrics & More | Article Recommendations | Supporting Information

ABSTRACT: Hexaferrites have a wide range of technological applications as well as a rich and complicated structural chemistry, with iron oxide layers inducing highly anisotropic ferrimagnetism that remains intact to high temperatures (>400 K). Most hexaferrites (i.e., M-type $BaFe_{12}O_{19}$) contain the dominant magnetic vectors normal to the hexagonal planes forming hard ferrimagnets, while the much less common Y-type investigated here typically contains the ferrimagnetic vectors in the iron oxide planes, creating soft ferrimagnets suitable for RF applications. To study the structural chemistry and magnetism of this less common hexaferrite phase, single crystals of $K_2Co_4V_9O_{22}$ (**I**) and $Ba_2Fe_{11}Ge_2O_{22}$ (**II**) were prepared. The structure of these compounds is a derivative of the sophisticated mineral greenwoodite, having a complex assembly of transition metal octahedra and tetrahedra, notably featuring Kagomé layers in spinel-type blocks that are magnetically isolated from one another. In particular, compound **II** provides a pathway to developing iron-rich hexaferrites where the magnetic ions are not diluted by site substitution of nonmagnetic ions. This results in an exceptionally high magnetic ordering temperature of 855 K to a canted antiferromagnetic state.

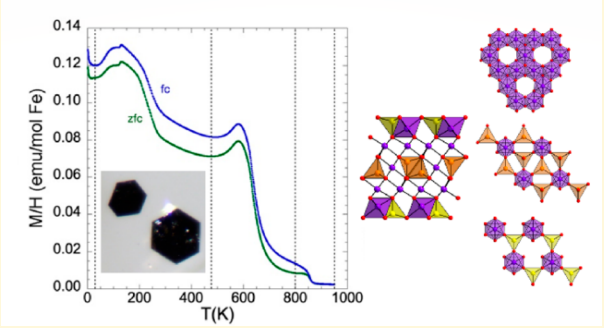

Downloaded via CLEMSON UNIV on December 16, 2021 at 23:18:44 (UTC).
See https://pubs.acs.org/sharingguidelines for options on how to legitimately share published articles.

1. INTRODUCTION

The hexaferrites are a relatively old class of compounds with a considerable history of practical application. They are relatively easy and inexpensive to prepare as powders on a commercial scale and have numerous useful technological properties.[1−3] They also have an exceptionally complex structural chemistry, and despite their importance, their structural details are not always well understood. Notwithstanding this complexity, they generally have a number of features in common. They are typically oxides with iron as the predominant magnetic ion, usually in the high spin Fe^{3+} state, although other first row magnetic ions can also be present. They also typically contain an alkaline earth ion, usually either Ba^{2+} or Sr^{2+}, which forms an oxide substructure separate from the structural units containing the magnetic ions. Their characteristic properties are highlighted by the fact that they order ferrimagnetically at relatively high temperatures (≥400 °C), so they are useful magnetic materials. They are often described using trade names ("Ferroxdure", "Ferroxplana") or generic labels such as "M-," "Y-," or "Z-" ferrites.[1−6]

Their useful and interesting magnetic behavior is derived from their tendency to form lattices with hexagonal substructures, wherein the planar ferrimagnetic structure imparts the magnetic behavior that can be manipulated appropriately for practical applications.[1−3] Hexagonal ferrites have also displayed room temperature multiferroic and magnetoelectric behavior, suggesting that they may have broader applications in quantum materials.[4] They can be divided into broad structural categories much like the planar perovskite derivatives (e.g., Ruddlesdon-Popper phases), where basic structural units are mixed and matched with interleaved layers in various combinations to form an extensive array of complex structure types.[1,7,8] The hexagonal layered nature of the ferrites introduces a strong magnetic anisotropy that is an important factor in many of their associated properties. Most commonly the magnetic vectors align perpendicular to the hexagonal layers, while more rarely, particularly in some materials containing divalent transition metal ions (Co^{2+}, Ni^{2+}), the magnetic vectors occur in the hexagonal plane.[1−3]

Of the wide range of ferrites, the most common class is the so-called M-type, with the general formula $MFe_{12}O_{19}$, where M is a divalent ion, usually Sr^{2+}, Ba^{2+}, or Pb^{2+}.[1,2] This material class found widespread use as hard ferrimagnets with relatively high coercivity and magnetic saturation values. A series of R-type ferrites, including $(Ba,Sr)M_{2\pm x}M'_{4\pm x}O_{11}$ (M = Mn, Fe,

Received: September 29, 2020
Revised: March 19, 2021
Published: April 1, 2021

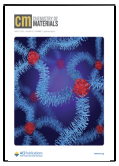

© 2021 American Chemical Society

https://doi.org/10.1021/acs.chemmater.0c03852
Chem. Mater. 2021, 33, 2258–2266

Co, Ni, Cu, Zn, Sn; M′ = Ru, Ti, Fe) have demonstrated a wide variety of magnetic characteristics, including high temperature ordering and spin glass behavior depending on the compositional and structural variations.[9−11] Another important structural class of hexaferrites is the so-called Y-type with the generic formula $Ba_2M_2Fe_{12}O_{22}$ (M = divalent transition metal). They represent one of the first classes of hexaferrites discovered and were given the trade name "Ferroxplana".[6,7] This phase is also sometimes called the QS phase. These are noteworthy in that they are one of the few hexaferrites where the magnetic vectors are oriented in the hexagonal plane and freely rotate within the *ab*-plane. As such they form soft ferrimagnetic materials and are useful for very high frequency (GHz) RF applications.[12−17]

The hexagonal layers of the Y-type (or QS) structures are part of a broader class of structures that contain Kagomé nets. These layers thus contain the appropriate symmetry for frustrated magnetism and possibly quantum spin behavior.[18−26] As with the layered perovskite derivatives, the hexagonal layers in the Y-type materials are separated by M^{2+}−O salt-like strata, creating structures with frustrated two-dimensional (2-D) magnetic layers that are only weakly coupled to other magnetically ordered layers.[27] An interesting series of studies were performed on some tin containing compounds of the QS phase, but the high temperature synthetic procedure and the demands of tin to be tetravalent and exclusively octahedral invariably led to mixed phases or disordered species, further complicating an already complex situation.[28,29] It should be noted that although the prototype M-hexaferrite $BaFe_{12}O_{19}$ can be grown as single crystals relatively straightforwardly,[30] most of the other hexaferrites, including the Y-phase, have only been synthesized and studied as powders or nanocrystallites.[31,32]

The Y (or QS) type materials also have a fascinating class of mineral analogues known as the greenwoodites.[33] The naturally occurring minerals are even more complex than the synthetic ferrites due to the variety of possible metal types, oxidation states, and coordination environments in the prototype structure. Of course, the natural minerals inevitably display an enormous range of different metal ion substitutions, disorder, and multiple oxidation states in the various samples. The parent greenwoodite itself illustrates all of these characteristics, with an elegant crystallographic analysis establishing an "ideal" structural model of $Ba_{1.20}(VOH)_{0.80}V_9Fe^{2+/3+}{}_2Si_2O_{22}$, with an actual experimentally determined composition of $Ba_{1.20}(VOH)_{0.80}(V_{8.33},Cr_{0.33},Ti_{0.13},Al_{0.13},Mn_{0.02})(Fe^{3+}{}_{1.08},Fe^{2+}{}_{0.60},Zn_{0.22},Al_{0.06},Mg_{0.04})(Si_{1.72},Fe^{3+}{}_{0.28})O_{22}$.[33] This tendency of natural minerals to incorporate a wide range of metal ions and oxidation states over disordered sites makes it challenging to study and interpret their physical properties. Their structural features, however, often do provide valuable inspiration for the development of related materials and new synthetic design.[34−39]

The structural complexity of the hexaferrites presents considerable challenges to the understanding of their physical properties. The scientific interest of the so-called $M_2M'_2Fe_{11}O_{22}$ Y- or QS-type compounds as potential quantum materials and their technological significance as high-frequency soft ferrimagnets make them attractive targets, however. We decided to employ the hydrothermal approach to see if well-ordered single crystals could be obtained for more detailed magnetic and physical property measurements. In this paper we report our initial efforts in preparing single crystals of two new QS-hexaferrrite analogues as well-formed single crystals, as well as preliminary magnetic studies that indicate high temperature magnetic ordering. The structural details are reported for well-ordered single crystals of the greenwoodite structure type for the first time, and the work is the first step in the detailed examination of this new class of potential 2-D Kagomé materials.

2. EXPERIMENTAL SECTION

2.1. Synthesis. $K_2Co_4V_9O_{22}$ (**I**) was synthesized from a 2:1:2 molar ratio of K_2CO_3 (0.0688 g, 0.498 mmol), CoO (0.0187 g, 0.249 mmol), and V_2O_5 (0.091 g, 0.498 mmol) in 0.4 mL of water. Reactants were loaded into a silver ampule that was subsequently sealed and placed in a Tuttle cold seal autoclave. The autoclave was heated to 580 °C for 7 days, generating 20 kpsi autogenous pressure. Crystals of the target compound formed as black hexagonal plates (Supporting Information, Figure S1) as about 50% of the total product, along with $K_2V_3O_8$. Semiquantitative analysis of metals (due to overlap of the oxygen signal with vanadium) in atomic percent (expected): V, 54.3 (60.0); Co, 34.2 (26.7); K, 11.5 (13.3) (SI, Figure S2).

$Ba_2Fe_{11}Ge_2O_{22}$ (**II**) was synthesized from a 4:11:4 molar ratio of BaO (0.061 g, 0.4 mmol), Fe_2O_3 (0.176 g, 1.1 mmol), and GeO_2 (0.042 g, 0.4 mmol) in 0.4 mL of 1 M KOH. Reactants were loaded into a silver ampule that was subsequently sealed and placed in a Tuttle cold seal autoclave. The autoclave was heated to 580 °C for 7 days, generating 20 kpsi autogenous pressure. Crystals of the target compound formed as a phase pure product of black hexagonal plates and microcrystals (SI, Figure S1), with an overall yield of 71% based on barium oxide. Elemental analysis in atomic percent (expected): O, 61.7 (59.4); Fe, 27.4 (29.7); Ge, 5.5 (5.4); Ba, 5.5 (5.4) (SI, Figure S3).

2.2. Structure Determination. Single crystal X-ray diffraction data were collected at room temperature using a Bruker D8 Venture diffractometer with Mo Kα (λ = 0.71073 Å) radiation from a microfocus source and a Photon 100 detector. Data were collected using phi and omega scans with a frame width of 0.5°. Data were processed (SAINT) and corrected for absorption (multiscan, SADABS) using the Apex 3 software package.[40] Space group determination (XPREP), structure solution by intrinsic phasing (SHELXT), and structure refinement by full-matrix least-squares techniques on F^2 (SHELXL) were performed using the SHELXTL suite.[41] All atoms were refined anisotropically. Optimization of the atom site identities was achieved through a series of test refinements, with the final site identities supported by the interatomic distances, anisotropic displacement parameters, bond valence sums, and elemental analysis by EDX. In this way optimized refinements were obtained using models with full site occupancy of individual constituent atoms, though we allow for the possibility of a small amount of substitutional disorder given the similar scattering factors of the transition metals involved. Crystallographic data is summarized in Table 1.

2.3. Magnetic Measurements. Magnetic properties were measured using a Quantum Design SQUID magnetometer (QD-MPMS3) equipped with an oven attachment. A 3.23 mg sample of single crystals of $Ba_2Fe_{11}Ge_2O_{22}$ were loaded into a massed silver pouch, which was then folded closed. The pouch was embedded in zircar cement on an oven sample rod. The sample was heated to 950 K, the applied field was oscillated to 0 Oe, and the sample was cooled to 300 K. The sample was then removed from the SQUID, unmounted from the oven sample rod, and glued to a quartz paddle using GE-7031 varnish. The sample was reinserted into the SQUID and cooled to 2 K. The magnetic susceptibility was measured in an applied field of 1000 Oe under zero-field-cooled conditions from 2 to 950 K with the sample being removed from the SQUID and reattached to the oven sample rod at 300 K. Susceptibility data under field-cooled conditions were then collected from 950 to 2 K with the sample being reattached to the quartz paddle at 300 K. The sample was then reheated to 950 K, and the magnetization as a function of

https://doi.org/10.1021/acs.chemmater.0c03852
Chem. Mater. 2021, 33, 2258−2266

Table 1. Crystallographic Data

empirical formula	$K_2Co_4V_9O_{22}$ (I)	$Ba_2Fe_{11}Ge_2O_{22}$ (II)
F.W. (g/mol)	1124.38	1386.21
temperature (K)	299(2)	300(2)
crystal system	trigonal	trigonal
space group	$P\bar{3}m1$	$P\bar{3}m1$
a (Å)	5.8392(3)	5.8532(3)
c (Å)	14.5176(8)	14.2601(7)
volume (Å^3)	428.68(5)	423.10(5)
Z	1	1
D(calcd) (g/cm^3)	4.355	5.440
μ, mm^{-1}	9.017	17.293
F(000)	529	638
crystal size (mm)	0.16 × 0.12 × 0.12	0.16 × 0.16 × 0.05
θ range, deg	2.81 to 26.50	2.86 to 30.53
reflections collected	6107	8960
independent reflections (R_{int})	398 (0.0285)	558 (0.0413)
no. of parameters	46	46
final R indices (obs. data)[a,b]	R_1 = 0.0213, wR_2 = 0.0601	R_1 = 0.0261, wR_2 = 0.0819
R indices (all data)[a,b]	R_1 = 0.0215, wR_2 = 0.0602	R_1 = 0.0264, wR_2 = 0.0818
goodness-of-fit on F^2	1.215	1.191

[a] $R_1 = \sum||F_o| - [F_c||/\sum|F_o|$. [b] $wR_2 = \{\sum[w(F_o^2 - F_c^2)^2]/\sum[wF_o^2]^2\}^{1/2}$.

the field from 5 T to −5 T to 5 T was collected at 950, 800, 475, 130, 115, and 30 K, again with measurements above 300 K being performed on an oven sample rod and below 300 K on a quartz paddle. All data were corrected for the diamagnetic contribution of the silver pouch. For the magnetic susceptibility data, the data below 300 K were normalized to the oven data by adding a correction factor to the data to set the 300 K data points equal. This correction is assumed to be the result of different diamagnetic contributions of the sample mounting methods and different sample radial offsets. The data were not corrected for the sample shape and radial offset effects, which can be appreciable (often several percent of the moment) in the MPMS3.[42] After all the measurements, the sample was removed from the silver pouch and analyzed via PXRD using a Bruker D2 Phaser equipped with a Cu Kα (λ = 1.5406 Å) source. Shown in Figure S4, no indication of the sample decomposition was observed, and the sample was found to be phase pure. Despite our best efforts to measure the magnetic properties of $K_2Co_4V_9O_{22}$, the presence of $K_2V_3O_8$ impurities and the relatively small crystal size of the target phase has prevented us from obtaining a sample of sufficient mass and purity for a meaningful magnetic measurement.

3. RESULTS AND DISCUSSION

3.1. Development of $K_2Co_4V_9O_{22}$ (I) and $Ba_2Fe_{11}Ge_2O_{22}$ (II) from Greenwoodite. Minerals can be an excellent source of inspiration for developing new materials having specific structural features to study their structure−property relationships. The compositional complexity of many natural species, however, often complicates the measurement and interpretation of their physical properties. Such is the case in natural greenwoodite, with its extraordinarily complex chemical composition.[33] Even in its more simplified ideal formula of $Ba_{1.20}(VOH)_{0.80}V_9Fe^{2+/3+}{}_2Si_2O_{22}$, the Ba/VOH disorder would complicate the magnetic behavior by introducing additional magnetically active V^{3+} ions into the otherwise nonmagnetic barium oxide layer. One attractive materials design strategy is to mimic that of the synthetic organic chemists who use natural products as inspiration for a jumping off point to make analogues with desirable properties. In this spirit we sought to prepare simplified compounds with the structural features of greenwoodite, including its 3-fold symmetric arrangements of magnetically active ions, but having more limited and well-defined distributions of ions (Table 2).

As a first step, we hoped to prepare a compound that did not contain the VOH disorder and eliminate the presence of trace elements such as Cr^{3+}, Al^{3+}, Ti^{4+}, Zn^{2+}, and Mg^{2+} that complicate the understanding of mineralogical greenwoodite. We previously found that the vanadate oxyanion, $(VO_4)^{3-}$, is an excellent tetrahedral building block for the formation of interesting magnetically ordered materials in hydrothermal conditions.[43−48] This led us to the preparation of $K_2Co_4V_9O_{22}$ (I) (Figure 1), which is isostructural with natural greenwoodite ($P\bar{3}m1$, a = 5.7500(6) Å, c = 14.4590(9) Å)[33] *via* several aliovalent substitutions. This includes the substitution of similarly sized ions K^+ for Ba^{2+}, V^{5+} for Si^{4+}, Co^{2+} for $Fe^{2+/3+}$, and Co^{2+} and V^{4+} at some of the V^{3+} sites. In this way the VOH disorder and trace impurity elements were eliminated. The chemical formula $K_2Co_4V_9O_{22}$ of compound I can then be rationalized as $K_2Co^{II}{}_2V^{III}{}_4V^{IV}{}_3O_6(Co^{II}O_4)_2(V^{V}O_4)_2$, which achieves charge neutrality and is consistent with the crystallographic observations, bond valence sums (Table 3), and elemental analysis. The presence of well-ordered Co^{2+}, V^{3+}, and V^{4+} at the octahedral sites comprising the transition metal network, however, still complicates the interpretation of any magnetic data. The partial *in situ* reduction of V^{5+} to V^{4+} and V^{3+} often occurs in hydrothermal systems,[49−51] and in this case is likely driven by the structural stability of these lower valence states in six-coordinate sites compared to four-coordinate sites[52] and the necessity of charge neutrality.

Having confirmed that the VOH disorder and trace elements were not essential to the formation of greenwoodite-type structures and that the structure type will tolerate modestly larger oxyanions (for example, the substitution of vanadate or germanate for silicate), we targeted an even simpler end member compound analogous to the theoretical barium end member $Ba_2V_9Fe_2Si_2O_{22}$.[33] Indeed, upon reconciling the structure of greenwoodite, Bartholomew and co-workers identified ferrites such as $Ba_2Sn_2MFe_{10-x}Ga_xO_{22}$ (M = divalent

Table 2. Crystal−Chemical Relationships between Greenwoodite,[33] $Ba_2Sn_2CoFe_{10}O_{22}$,[29] $K_2Co_4V_9O_{22}$ (I, This Work), and $Ba_2Fe_{11}Ge_2O_{22}$ (II, This Work)

structural component	multiplicity	greenwoodite	QS-type $Ba_2Sn_2CoFe_{10}O_{22}$	$K_2Co_4V_9O_{22}$ (I)	$Ba_2Fe_{11}Ge_2O_{22}$ (II)
interlayer site	2	Ba^{2+}, V^{3+}OH	Ba^{2+}	K^+	Ba^{2+}
octahedral site 1 (Oh1)	2	V^{3+}, Cr^{3+}, Al^{3+}, Ti^{4+}	Sn^{4+}, Co^{2+}, Fe^{3+}	Co^{2+}	Fe^{3+}
Octahedral site 2 (Oh2)	6	V^{3+}, Cr^{3+}, Al^{3+}, Ti^{4+}	Co^{2+}, Fe^{3+}	V^{3+}, V^{4+}	Fe^{3+}
octahedral site 3 (Oh3)	1	V^{3+}, Cr^{3+}, Al^{3+}, Ti^{4+}	Sn^{4+}, Co^{2+}, Fe^{3+}	V^{4+}	Fe^{3+}
tetrahedral metal 4 (Td1)	2	Fe^{3+}, Fe^{2+}, Zn^{2+}, Mg^{2+}	Co^{2+}, Fe^{3+}	Co^{2+}	Fe^{3+}, Fe^{2+}
tetrahedral oxyanion 5 (Td2)	2	Si^{4+}, Fe^{3+}	Fe^{3+}	V^{5+}	Ge^{4+}

https://doi.org/10.1021/acs.chemmater.0c03852
Chem. Mater. 2021, 33, 2258−2266

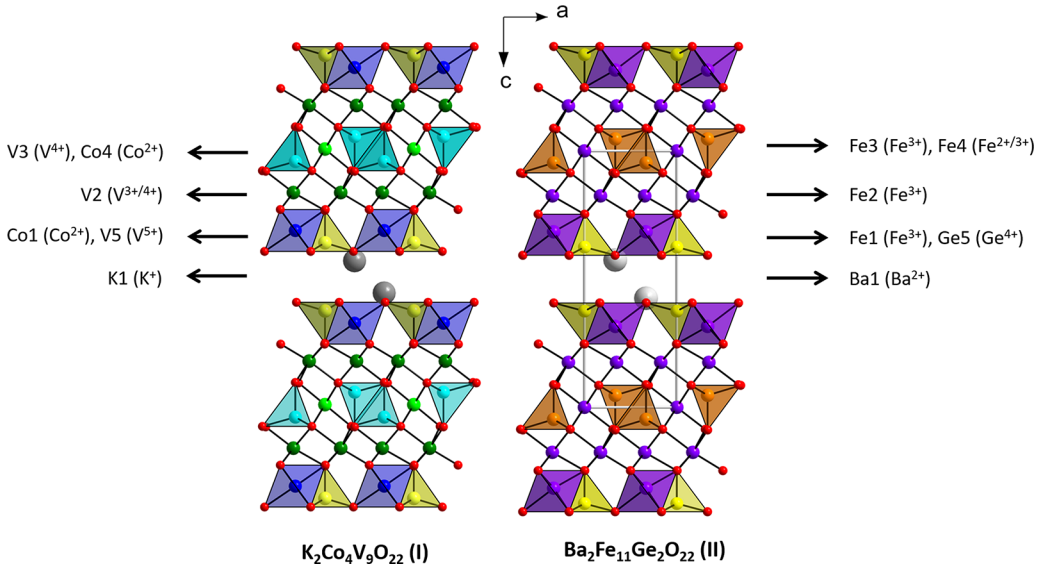

Figure 1. Structure of $K_2Co_4V_9O_{22}$ (**I**, left) and $Ba_2Fe_{11}Ge_2O_{22}$ (**II**, right) viewed along the *b*-axis. For **I**, octahedral $V^{3+/4+}$ sites are shown in dark green, octahedral V^{4+} sites are shown in light green, tetrahedral V^{5+} sites are shown in yellow, octahedral Co^{2+} sites are shown in blue, tetrahedral Co^{2+} sites are shown in cyan, K atoms are shown in gray, and O atoms are shown in red. For **II**, octahedral Fe atoms are shown in purple, tetrahedral Fe atoms are shown in orange, Ge atoms are shown in yellow, Ba atoms are shown in silver, and O atoms are shown in red.

transition metal) and $Ba_2Sn_2MFe_{10}O_{22}$ as being analogous to the mineral.[28,29,33] The interest in ferrite materials led us to seek a further simplified isostructural compound, $Ba_2Fe_{11}Ge_2O_{22}$, consisting of an electronically silent germanate oxyanion ($(GeO_4)^{4-}$) with a single transition metal, iron, occupying all the transition metal sites. This represents a straightforward composition and distribution of elements, where Fe^{3+} occupies all of the octahedral sites (Oh1, Oh2, Oh3), $Fe^{2+/3+}$ occupies the transition metal tetrahedral site (Td1), and the nonmagnetic Ge^{4+} comprises the other tetrahedral oxyanion site (Td2). As such the $Ba_2Fe_{11}Ge_2O_{22}$ material is a particularly attractive candidate for magnetic studies, with well-formed single crystals obtained in the present study enabling oriented magnetic studies.

3.2. Structural Characteristics of $K_2Co_4V_9O_{22}$ and $Ba_2Fe_{11}Ge_2O_{22}$. The structural features of both compounds can best be described using $Ba_2Fe_{11}Ge_2O_{22}$ as the structural archetype. The layered structure consists of iron germanate slabs in the *ab* plane, connected along the *c*-axis through barium oxide layers (Figure 1). The iron germanate slabs can be further subdivided into individual layers within the slab (Figure 2). At the center of the slabs are octahedral Fe^{3+} (Fe3) and tetrahedral $Fe^{2+/3+}$ (Fe4) sites, connected to one another in a corner sharing fashion. These layers are bound on the top and bottom by Kagomé layers of Fe^{3+} (Fe2) that are constructed of edge-shared octahedra. The Kagomé layers are connected to the central layer via edge sharing between Fe3 and Fe2 and corner sharing between Fe4 and Fe2. The slabs are terminated on the top and bottom by a third layer, comprised of octahedral Fe^{3+} (Fe1) and the nonmagnetic tetrahedral oxyanion (Ge5). These layers connect to the Kagomé layers via corner sharing of Fe2 with Fe1 and corner sharing of Fe2 with Ge5.

The compound crystallizes in space group $P\bar{3}m1$, so there are inherent 3-fold symmetric features that can impart interesting magnetic properties such as frustration.[27] Tetrahedral oxyanions including $(SiO_4)^{4-}$, $(GeO_4)^{4-}$, $(VO_4)^{3-}$, and $(MoO_4)^{2-}$ have proven useful as building blocks for the formation of trigonal symmetry features in several systems, as they can align above and below the gaps in edge sharing triangular and hexagonal transition metal substructures according to the 3-fold axes of the tetrahedra (Figure 3).[22,27,35,54−57] In the present structure type, the Kagomé layer of Fe2 octahedra is of note (Figure 4a). While the individual Fe2 sites possess only mirror symmetry, their relation to one another forms a Kagomé net of two different equilateral triangles with Fe−Fe distances of 2.804(2) Å and 3.049(2) Å. The Fe3/Fe4 layer also has 3-fold symmetry, created by the orientation of the triangular faces of the Fe3 octahedra and the basal face of the Fe4 tetrahedra (where the apical Fe4−O1 bond is aligned with the *c*-axis). Although there are no edge sharing interactions between Fe atoms within this layer, its triangular symmetry remains important to facilitate edge sharing interactions (Fe−Fe = 3.059(6) Å) between this layer and the Kagomé layer. The sandwich of the Fe3/Fe4 layer between two Kagomé layers forms the basis for a spinel-like arrangement of octahedra (Figure 4b). It is this interaction of strong *intra* layer coupling with weak *inter* layer coupling, as highlighted by Hageman et al.,[27] that is one factor that makes Kagomé systems such as this attractive to study. The tetrahedral Fe4 site occupies gaps in this edge sharing framework, which can also be thought of as a slab of interlocked cubes whose corners are formed from iron and oxygen atoms (Figure 4c). The Fe1/Ge5 layer similarly also has 3-fold symmetry as it fuses to the opposing side of the Kagomé layer, with the octahedra and tetrahedra aligned to have triangular faces in the *ab* plane.

The isostructural $K_2Co_4V_9O_{22}$ (**I**) follows the same layered arrangement in the space group $P\bar{3}m1$, with a somewhat more complex distribution of V^{5+}, V^{4+}, V^{3+}, and Co^{2+} transition metal ions (Figure 1). The central layer of the slab is a corner sharing arrangement of V3 (V^{4+}) octahedra and Co4 (Co^{2+}) tetrahedra. The Kagomé layers that sandwich the central layer are entirely composed of edge-shared V2 octahedra, with the mixed-valence V^{3+} and V^{4+} ions distributed throughout the V2 sites providing an average charge of +3.33. The V−V distances

https://doi.org/10.1021/acs.chemmater.0c03852
Chem. Mater. 2021, 33, 2258−2266

Table 3. Interatomic Distances (Å) and Bond Valence Sums (b.v.s., in Valence Units) for $K_2Co^{II}_2V^{III}_4V^{IV}_3O_6(Co^{II}O_4)_2(V^{V}O_4)_2$ and $Ba_2Fe^{III}_9O_6((Fe^{II/III})O_4)_2(GeO_4)_2$[a]

$K_2Co_4V_9O_{22}$, $K_2Co^{II}_2V^{III}_4V^{IV}_3O_6(Co^{II}O_4)_2(V^{V}O_4)_2$			$Ba_2Fe_{11}Ge_2O_{22}$, $Ba_2Fe^{III}_9O_6((Fe^{II/III})O_4)_2(GeO_4)_2$		
	length (Å)	b.v.s.		length (Å)	b.v.s.
Co1−O4	2.083(3)	0.348	Fe1−O4	1.965(6)	0.536
Co1−O4	2.083(3)	0.348	Fe1−O4	1.965(6)	0.536
Co1−O4	2.083(3)	0.348	Fe1−O4	1.965(6)	0.536
Co1−O5	2.112(3)	0.321	Fe1−O5	2.140(5)	0.334
Co1−O5	2.113(3)	0.321	Fe1−O5	2.140(5)	0.334
Co1−O5	2.113(3)	0.321	Fe1−O5	2.140(5)	0.334
∑(b.v.s.)		2.01	∑(b.v.s.)		2.79
V2−O1	1.986(3)	0.519	Fe2−O1	2.041(6)	0.467
V2−O2	2.066(3)	0.418	Fe2−O2	2.034(4)	0.476
V2−O3	2.077(2)	0.405	Fe2−O3	2.104(4)	0.394
V2−O3	2.077(2)	0.405	Fe2−O3	2.104(4)	0.394
V2−O4	1.886(2)	0.679	Fe2−O4	1.937(4)	0.618
V2−O4	1.886(2)	0.679	Fe2−O4	1.937(4)	0.618
∑(b.v.s.)		3.11 (3.47)[b]	∑(b.v.s.)		2.97
V3−O3	1.941(3)	0.654	Fe3−O3	1.987(5)	0.54
V3−O3	1.941(3)	0.654	Fe3−O3	1.987(5)	0.54
V3−O3	1.941(3)	0.654	Fe3−O3	1.987(5)	0.54
V3−O3	1.941(3)	0.654	Fe3−O3	1.987(5)	0.54
V3−O3	1.941(3)	0.654	Fe3−O3	1.987(5)	0.54
V3−O3	1.941(3)	0.654	Fe3−O3	1.987(5)	0.54
∑(b.v.s.)		3.92	∑(b.v.s.)		3.24
Co4−O1	1.972(5)	0.469	Fe4−O1	1.925(10)	0.597
Co4−O3	1.945(3)	0.505	Fe4−O3	1.897(5)	0.644
Co4−O3	1.945(3)	0.505	Fe4−O3	1.897(5)	0.644
Co4−O3	1.945(3)	0.505	Fe4−O3	1.897(5)	0.644
∑(b.v.s.)		1.98	∑(b.v.s.)		2.529 (2.71)[c]
V5−O5	1.695(3)	1.34	Ge5−O5	1.745(6)	1.01
V5−O5	1.695(3)	1.34	Ge5−O5	1.745(6)	1.01
V5−O5	1.695(3)	1.34	Ge5−O5	1.745(6)	1.01
V5−O2	1.831(5)	0.927	Ge5−O2	1.829(8)	0.803
∑(b.v.s.)		4.95	∑(b.v.s.)		3.83

[a]The b.v.s. for vanadium were calculated with the bond valence parameter of 1.743 for V^{3+} (V2), 1.784 for V^{4+}(V2[a], V3), and 1.803 for V^{5+}(V5). The b.v.s. for iron were calculated with the bond valence parameter of 1.734 for Fe^{2+}(Fe4) and 1.759 for Fe^{3+}(Fe1, Fe2, Fe3, Fe4[b]). The bond valence sums for cobalt and germanium were calculated with a bond valence parameter of 1.692 for Co^{2+} (Co1, Co4) and 1.748 for Ge^{4+} (Ge5).[53] [b]Bond valence parameter of 1.784 for V^{4+}. [c]Bond valence parameter of 1.759 for Fe^{3+}.

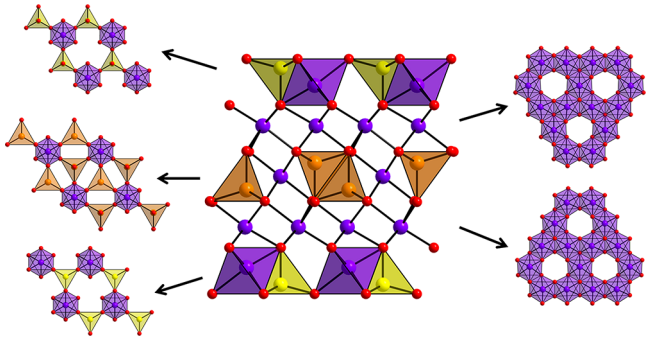

Figure 2. Layered substructures comprising the iron germanate slabs in $Ba_2Fe_{11}Ge_2O_{22}$. The slab substructure is viewed along the *b*-axis, while the individual layer substructures are viewed along the *c*-axis. Octahedral Fe atoms are shown in purple, tetrahedral Fe atoms are shown in orange, Ge atoms are shown in yellow, and O atoms are shown in red.

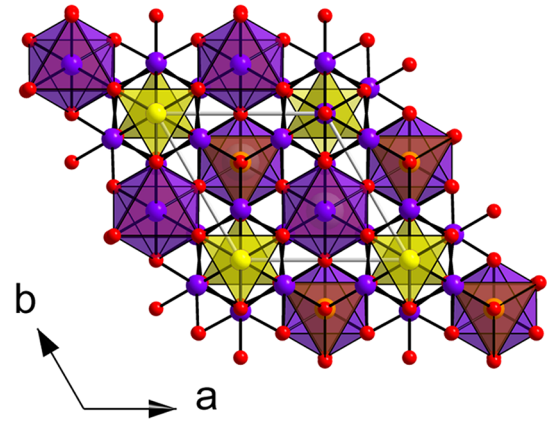

Figure 3. Structure of $Ba_2Fe_{11}Ge_2O_{22}$ viewed along the *c*-axis. Color scheme is the same as in Figure 2. The 3-fold axes of the $(GeO_4)^{4-}$ tetrahedra align with gaps in the Kagomé layer to template the slabs.

of the equilateral triangles in these Kagomé layers are 2.7277(12) Å and 3.1115(12) Å, with a V2−V3 distance of 3.0563(7) Å through the edge-shared connection between the Kagomé layers and the interstitial layer sandwiched between them. The terminal layers of the slabs contain octahedral Co1 (Co^{2+}) sites corner sharing with the tetrahedral V5 (V^{5+}) sites.

https://doi.org/10.1021/acs.chemmater.0c03852
Chem. Mater. 2021, 33, 2258−2266

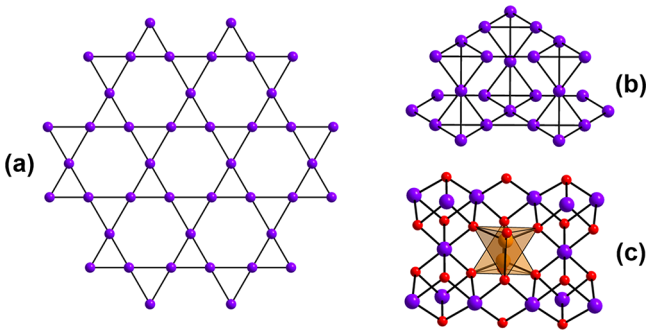

Figure 4. Triangular lattices in $Ba_2Fe_{11}Ge_2O_{22}$: (a) edge sharing connections between Fe2 atoms forming the Kagomé layer, (b) edge sharing connections between Fe2 and Fe3 atoms forming the spinel-like substructure, and (c) iron oxide cubes with gaps filled by Fe(4) tetrahedra in the spinel-like substructure.

The larger *c*-axis lattice parameter of $K_2Co_4V_9O_{22}$ compared to $Ba_2Fe_{11}Ge_2O_{22}$ is largely attributed to the presence of K^+ versus Ba^{2+} between the slabs, where K−O bond lengths (2.938(4) Å to 3.351(4) Å) are longer than the equivalent Ba−O bond lengths (2.928(5) Å to 3.048(5) Å).

While isostructural with the greenwoodite structure type as described above, given the magnetic studies below, structures **I** and **II** are also aptly described as hexagonal QS ferrites. In the QS-type structures, spinel-like blocks (S) alternate with Q layers along the *c*-axis. The spinel block consists of the octahedra that form two-dimensional edge sharing interactions, namely, those of the central layer and the two Kagomé layers that sandwich it. The Q-block provides a magnetically insulating layer separating the spinel blocks,[27] since connections between octahedra in the Q and S blocks occur only through corner sharing. The barium oxide layers within the Q-block provide a rather large separation between the magnetic S blocks along the *c*-axis, enhancing the insulating effect and leading to only weak magnetic coupling between the layers. In earlier work similar structures have been obtained using significant amounts of Sn at the octahedral site occupied by Fe1 in the case of $Ba_2Fe_{11}Ge_2O_{22}$, such as in $Ba_2Sn_2MFe_{10}O_{22}$ (M = Mg, Mn, Ni, Co, Cu, Zn, Cd).[28,29,58,59] The presence of tetravalent Sn^{4+} leads to the introduction of a wide range of divalent metals listed above. These are present in varying degrees in both tetrahedral and octahedral sites, including those in the spinel block. In some cases more extensive substitution of nonmagnetic ions such as Zn^{2+} and Ga^{3+} occurs at the tetrahedral sites to further isolate the magnetic layers, as demonstrated by $Ba_2Sn_2Ga_3ZnCr_7O_{22}$.[27,60,61] In the case of $Ba_2Fe_{11}Ge_2O_{22}$, all of the edge sharing sites comprising the spinel layer are occupied by Fe^{3+}, making the understanding of the structure more internally consistent. In $K_2Co_4V_9O_{22}$, the spinel block is comprised of a mixed-valence vanadium site in the Kagomé layer (average charge of +3.33) and a V^{4+} site in the sandwiched layer containing the octahedral V3 site and tetrahedral Co4 site. As such the description of the formal magnetic sites would be expected to be far more complex than even the ferrite structure in **II** (below).

3.3. Magnetic Properties of $Ba_2Fe_{11}Ge_2O_{22}$. The magnetic properties of QS ferrites vary greatly based on which sites are occupied by magnetic ions. The Kagomé lattices within the S layer are a well-known geometry that can lead to magnetic frustration. While no QS ferrites are known whereby *only* the Kagomé sublattice is occupied by magnetic ions, further occupancy of the Oh2 sites by magnetic ions does not relieve this frustration. This is the case in $Ba_2Sn_2Ga_3ZnCr_7O_{22}$, which was found to be highly frustrated, entering a spin-glass state at 1.5 K despite a Curie−Weiss theta value of −312 K.[27] The addition of magnetic ions to other sites reduces the symmetry and relieves this frustration, which results in magnetic ordering at high temperatures. For example, the series $Ba_2Sn_2MFe_{10-x}Ga_xO_{22}$ (M = Mg, Ni, Co, Cu) were found to order ferrimagnetically with ordering temperatures between 334 and 444 K.[29] In these compounds, magnetic ions predominantly or fully occupy both tetrahedral sites and the Oh2 and Oh3 sites which leads to the ferrimagnetic interaction. The nonmagnetic Sn occupies the Oh1 site, and in some cases a small percentage of magnetic ion is also mixed onto this site. Compound **II** differs from the $Ba_2Sn_2MFe_{10-x}Ga_xO_{22}$ series in that the nonmagnetic ion resides exclusively on the Td2 site, and there is no apparent mixing of nonmagnetic ions onto any of the magnetic sites, with the only site mixing being the mixed-valence $Fe^{2+/3+}$ at the Td1 site. In this sense the magnetic ion arrangement is "pure" compared to most hexagonal ferrites. Because magnetic ions reside on the Td1 and Oh3 sites along with the Kagomé (Oh2) and Oh1 sites, the magnetic frustration is expected to be relieved in $Ba_2Fe_{11}Ge_2O_{22}$, allowing for high temperature ordering.

The magnetic properties of $Ba_2Fe_{11}Ge_2O_{22}$ are shown in Figure 5 and Figure S5. The magnetic susceptibility exhibits ordering at a very high temperature, T = 855 K with a spin reorientation at T = 631 K, both of which are characterized by increases in the magnetic susceptibility. The magnetization as a function of the field at 800 K exhibits a small jump at low fields

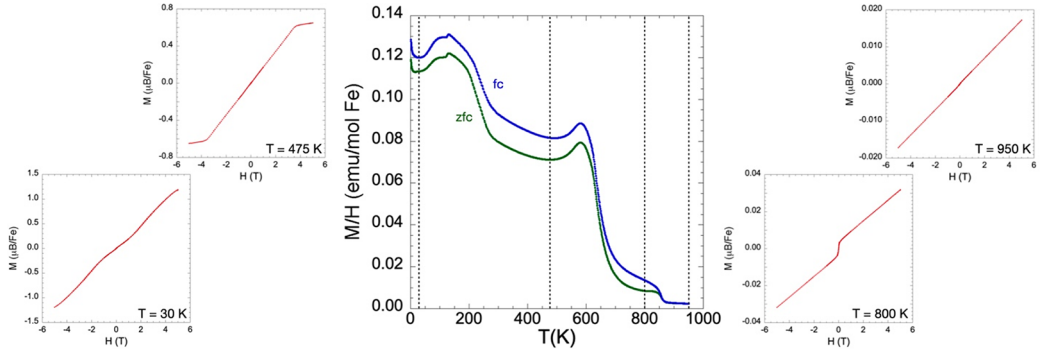

Figure 5. Magnetic susceptibility and magnetization as a function of the field for $Ba_2Fe_{11}Ge_2O_{22}$. The dotted lines in the susceptibility indicate the temperatures of the field sweep measurements. For a larger figure including all measured field sweeps and the inverse susceptibility, see Figure S5.

https://doi.org/10.1021/acs.chemmater.0c03852
Chem. Mater. 2021, 33, 2258−2266

with no hysteresis. The small magnitudes of both the increase in susceptibility and the jump in the magnetization, along with the lack of hysteresis, suggest that the ordering at 855 K is to a canted antiferromagnetic state. Neutron diffraction measurements will be necessary to confirm the nature of the magnetic ordering and to determine the nature of the spin reorientation. The higher magnetic ordering temperature of **II** relative to the $Ba_2Sn_2MFe_{10-x}Ga_xO_{22}$ series can be attributed to the isolation of the magnetic layers by the nonmagnetic germanates as well as a lack of nonmagnetic ion mixing onto the magnetic sites. Other hexaferrites exhibiting relatively high temperature ordering include $Ba_2Co_2Fe_{12}O_{22}$ at 613 K,[62] $Ba_2Co_{1.5}Ni_{0.5}Fe_{12}O_{22}$ at 718 K,[63] and $BaSrCo_2Fe_{11}AlO_{22}$ at 760 K.[64] The exceptionally high ordering temperature of 855 K in $Ba_2Fe_{11}Ge_2O_{22}$ is in line with that observed in some other Fe rich ferrites. For example, $BaFe_4O_7$ was found to undergo a canted antiferromagnetic ordering with T_N = 850 K.[65] It was further confirmed that the magnetic behavior of **II** at high temperatures is not due to any new phase formation, as PXRD after all magnetic measurements were performed demonstrates that the structure of **II** remains intact.

4. CONCLUSIONS

Two new hexagonal ferrites, $K_2Co_4V_9O_{22}$ (**I**) and $Ba_2Fe_{11}Ge_2O_{22}$ (**II**), were prepared having the Y- or QS-type structures featuring metal oxide layers with Kagomé net components imparting two-dimensional magnetic behavior. The compounds were grown as high-quality single crystals to enable future detailed magnetic structure studies. This particular structure type is also adopted by the mineral greenwoodite. The study provides a pathway employing synthetic chemical tools and aliovalent substitutions to access materials of interest that have simpler chemical compositions than their mineralogical counterparts, while retaining key structural features that impart unusual magnetic properties. In this case, **I** and **II** both contain well-ordered sites based on simplified chemistry compared to greenwoodite and the related QS ferrites. The structures generally consist of two types of layers, where significant intralayer magnetic coupling is enabled by edge-shared octahedra of magnetically active ions, with weaker intralayer coupling occurring through corner sharing interactions and magnetically inactive ions. The development of compound **II**, having fully occupied iron at the octahedral sites and one tetrahedral site, and nonmagnetic germanium at the second tetrahedral site, allows the magnetic properties of this type of magnetic ferrite to be studied for the first time. Our initial magnetic study indicates that the magnetic and nonmagnetic ions in $Ba_2Fe_{11}Ge_2O_{22}$ are distributed in a way that results in high temperature ordering at 855 K to a canted antiferromagnetic state, much higher than the ferrimagnetic transitions of similar ferrites which are diluted by substitutional disorder of nonmagnetic Sn^{4+} ions (334−444 K). The ability to prepare single crystals with ordered sites in highly magnetically anisotropic systems will enable more detailed oriented magnetic and neutron studies of these complex, interesting species.

■ ASSOCIATED CONTENT

Supporting Information

The Supporting Information is available free of charge at https://pubs.acs.org/doi/10.1021/acs.chemmater.0c03852.

Optical micrographs, elemental analysis by EDX, PXRD patterns, and magnetic data (PDF)

X-ray crystallographic data (CIF)

■ AUTHOR INFORMATION

Corresponding Author

Joseph W. Kolis − *Department of Chemistry and Center for Optical Materials Science and Engineering Technologies (COMSET), Clemson University, Clemson, South Carolina 29634-0973, United States*; Email: kjoseph@clemson.edu

Authors

Megan M. Smart − *Department of Chemistry and Center for Optical Materials Science and Engineering Technologies (COMSET), Clemson University, Clemson, South Carolina 29634-0973, United States*

Tiffany M. Smith Pellizzeri − *Department of Chemistry and Center for Optical Materials Science and Engineering Technologies (COMSET), Clemson University, Clemson, South Carolina 29634-0973, United States; Department of Chemistry and Biochemistry, Eastern Illinois University, Charleston, Illinois 61920, United States;* orcid.org/0000-0002-1525-9352

Gregory Morrison − *Department of Chemistry and Biochemistry, University of South Carolina, Columbia, South Carolina 29208, United States;* orcid.org/0000-0001-9674-9224

Colin D. McMillen − *Department of Chemistry and Center for Optical Materials Science and Engineering Technologies (COMSET), Clemson University, Clemson, South Carolina 29634-0973, United States;* orcid.org/0000-0002-7773-8797

Hans-Conrad zur Loye − *Department of Chemistry and Biochemistry, University of South Carolina, Columbia, South Carolina 29208, United States;* orcid.org/0000-0001-7351-9098

Complete contact information is available at: https://pubs.acs.org/10.1021/acs.chemmater.0c03852

Notes

The authors declare no competing financial interest.

■ ACKNOWLEDGMENTS

The synthetic and structural work done at Clemson University was supported by the National Science Foundation, DMR-1808371. For the magnetic measurements done at the University of South Carolina, DOE Award DE-SC0016574 is acknowledged.

■ REFERENCES

(1) Pullar, R. C. Hexagonal ferrites: A review of the synthesis, properties and applications of hexaferrite ceramics. *Prog. Mater. Sci.* **2012**, *57*, 1191−1334.

(2) Kimura, T. Magnetoelectric Hexaferrites,. *Annu. Rev. Condens. Matter Phys.* **2012**, *3*, 93−110.

(3) Ozgur, U.; Alivov, Y.; Morkoc, H. Microwave ferrites, part 1: fundamental properties,. *J. Mater. Sci.: Mater. Electron.* **2009**, *20*, 789−834.

(4) Kitagawa, Y.; Hiraoka, Y.; Honda, T.; Ishikura, T.; Nakamura, H.; Kimura, T. Low-field magnetoelectric effect at room temperature,. *Nat. Mater.* **2010**, *9*, 797−802.

(5) Jonker, G. H.; Wijn, H. P. J.; Braun, P. B. Magnetic and microwave absorbing properties of m-type hexaferrites substituted by Ru-Co ($BaFe_{12-2x}Ru_xCo_xO_{19}$). *Philips Technol. Rev.* **1956**, *18*, 145.
(6) Stuijts, A. L.; Wijn, H. P. J. Crystal Oriented Ferroxplana. *Philips Technol. Rev.* **1957**, *19*, 209−244.
(7) Delacotte, C.; Whitehead, G. F. S.; Pitcher, M. J.; Robertson, C. M.; Sharp, P. M.; Dyer, M. S.; Alaria, J.; Claridge, J. B.; Darling, G. R.; Allan, D. R.; Winter, G.; Rosseinsky, M. J. Structure determination and crystal chemistry of large repeat mixed-layer hexaferrites,. *IUCrJ* **2018**, *5*, 681−698.
(8) Kohn, J. A.; Eckart, D. W.; Cook, C. F. Crystallography of the Hexagonal Ferrites,. *Science* **1971**, *172*, 519−525.
(9) Shlyk, L.; Strobel, S.; Farmer, B.; De Long, L. E.; Niewa, R. Coexistence of ferromagnetism and unconventional spin-glass freezing in the site-disordered kagome ferrite $SrSn_2Fe_4O_{11}$,. *Phys. Rev. B: Condens. Matter Mater. Phys.* **2018**, *97*, 054426.
(10) Shlyk, L.; De Long, L. E.; Niewa, R. Structure and physical properties of $SrNiRu_5O_{11}$ single crystals: An R-type ferrite based on ordered kagome nets,. *Phys. Rev. B: Condens. Matter Mater. Phys.* **2017**, *95*, 024433.
(11) Foo, M. L.; Huang, Q.; Lynn, J. W.; Lee, W.-L.; Klimczuk, T.; Hagemann, I. S.; Ong, N. P.; Cava, R. J. Synthesis, structure and physical properties of Ru ferrites: $BaMRu_5O_{11}$ (M = Li and Cu) and $BaM'_2Ru_4O_{11}$ (M' = Mn, Fe and Co),. *J. Solid State Chem.* **2006**, *179*, 563−572.
(12) Stergiou, C. A.; Litsardakis, G. Y-type hexagonal ferrites for microwave absorber and antenna applications,. *J. Magn. Magn. Mater.* **2016**, *405*, 54−61.
(13) Bai, Y.; Zhou, J.; Gui, Z.; Yue, Z.; Li, L. Complex Y-type hexagonal ferrites: an ideal material for high-frequency chip magnetic components. *J. Magn. Magn. Mater.* **2003**, *264*, 44−49.
(14) Zenger, M. New Developments in the field of soft magnetic ferrites. *J. Magn. Magn. Mater.* **1992**, *112*, 372−376.
(15) You, J.-H.; Yoo, S.-I. Magnetic properties of Zn-substituted Y-type hexaferrites, $Ba_2Zn_xFe_{2-x}Fe_{12}O_{22}$,. *J. Magn. Magn. Mater.* **2019**, *471*, 255−261.
(16) You, J.-H.; Choi, S.; Park, S.-Y.; Yoo, S. I. Enhanced microwave absorption properties of Zn-substituted Y-type hexaferrites. *J. Magn. Magn. Mater.* **2019**, *491*, 165640.
(17) Zhai, K.; Su, N.; Sun, J.; Cheng, J.; Liu, Z.; Sun, Y. Pressure effect on spin-driven multiferroicity in a Y-type hexaferrite,. *J. Mater. Chem. C* **2019**, *7*, 4173−4177.
(18) Nocera, D. G.; Bartlett, B. M.; Grohol, D.; Papoutsakis, D.; Shores, M. P. Spin Frustration in 2-D Kagome Lattices: A Problem for Inorganic Synthetic Chemistry,. *Chem. - Eur. J.* **2004**, *10*, 3850−3859.
(19) Trump, B. A.; Koohpayeh, S. M.; Livi, K. J. T.; Wen, J.-J.; Arpino, K. E.; Ramasse, Q. M.; Brydson, R.; Feygenson, M.; Takeda, H.; Takigawa, M.; Kimura, K.; Nakatsuji, S.; Broholm, C. L.; McQueen, T. M. Universal geometric frustration in pyrochlores. *Nat. Commun.* **2018**, *9*, 2619.
(20) Puphal, P.; Zoch, K. M.; Desor, J.; Bolte, M.; Krellner, C. Kagome quantum spin systems in the atacamite family,. *Phys. Rev. Mater.* **2018**, *2*, 063402.
(21) Norman, M. R. Herbertsmithite and the Search for the Quantum Spin Liquid,. *Rev. Mod. Phys.* **2016**, *88*, 041002.
(22) Smith Pellizzeri, T. M.; McMillen, C. D.; Kolis, J. W. Alkali Transition-Metal Molybdates: A Stepwise Approach to Geometrically Frustrated Systems,. *Chem. - Eur. J.* **2020**, *26*, 597−600.
(23) Wen, J.-J; Lee, Y. S. The Search for the Quantum Spin Liquid in Kagome Antiferromagnets,. *Chin. Phys. Lett.* **2019**, *36*, 050101.
(24) Bojesen, T. A.; Onoda, S. Quantum spin ice under a [111] magnetic field: from pyrochlore to kagome,. *Phys. Rev. Lett.* **2017**, *119*, 227204.
(25) Lhotel, E.; Petit, S.; Ciomaga Hatnean, M.; Ollivier, J.; Mutka, H.; Ressouche, E.; Lees, M. R.; Balakrishnan, G. Evidence for dynamic kagome ice. *Nat. Commun.* **2018**, *9*, 3786.
(26) Sanders, M. B.; Krizan, J. W.; Cava, R. J. $RE_3Sb_3Zn_2O_{14}$ (RE = La, Pr, Nd, Sm, Eu, Gd): a new family of pyrochlore derivatives with rare earth ions on a 2D Kagome lattice,. *J. Mater. Chem. C* **2016**, *4*, 541−550.
(27) Hageman, I. S.; Huang, Q.; Gao, X. P. A.; Ramirez, A. P.; Cava, R. J. Geometric Magnetic Frustration in $Ba_2Sn_2Ga_3ZnCr_7O_{22}$: A Two-Dimensional Spinel Based Kagomé Lattice,. *Phys. Rev. Lett.* **2001**, *86*, 864−897.
(28) Cadee, M. C.; Ijdo, D. J. W. The Six Layer Structure of $BaSn_{0.9}Fe_{5.47}O_{11}$. *J. Solid State Chem.* **1981**, *40*, 290−300.
(29) Cadee, M. C.; de Groot, H J. M.; de Jongh, L. J.; Ijdo, D. J. W. Crystal Structure and Magnetic Properties of Some New Hexagonal Ferrites $Ba_2Sn_2MeFe_{10-x}Ga_xO_{22}$ with the QS- Structure,. *J. Magn. Magn. Mater.* **1986**, *62*, 367−380.
(30) Cao, H. B.; Zhao, Z. Y.; Lee, M.; Choi, E. S.; McGuire, M. A.; Sales, B. C.; Zhou, H. D.; Yan, J.-Q.; Mandrus, D. G. High pressure floating zone growth and structural properties of ferrimagnetic quantum paraelectric $BaFe_{12}O_{19}$. *APL Mater.* **2015**, *3*, 062512.
(31) Alizad Farzin, Y.; Mirzaee, O.; Ghasemi, A. Synthesis behavior and magnetic properties of Mg-Ni co-doped Y-type hexaferrite prepared by sol-gel auto-combustion method,. *Mater. Chem. Phys.* **2016**, *178*, 149−159.
(32) Murtaza, G.; Ahmad, R.; Hussain, T.; Ayub, R.; Ali, I.; Khan, M. A.; Akhtar, M. N. Structural and magnetic properties of Nd−Mn substituted Y-type hexaferrites synthesized by microemulsion method. *J. Alloys Compd.* **2014**, *602*, 122−129.
(33) Bartholomew, P. R.; Mancini, F.; Harlow, G. E.; Deifel, N.; Cahill, C.; Bernhardt, H.-J. Greenwoodite, a New Nesosilicate from British Columbia with a Ba-VOH Coupled Substitution and Tetrahedral Fe: Description and Structure. *Can. Mineral.* **2012**, *50*, 1233−1242.
(34) McMillen, C. D.; Kolis, J. W. Hydrothermal synthesis as a route to mineralogically-inspired structures,. *Dalton Trans.* **2016**, *45*, 2772−2784.
(35) Sanjeewa, L. D.; McMillen, C. D.; Willett, D.; Chumanov, G.; Kolis, J. W. Hydrothermal Synthesis of Single Crystals of Transition Metal Vanadates in the Glaserite Phase,. *J. Solid State Chem.* **2016**, *236*, 61−68.
(36) Malcherek, T.; Welch, M. D.; Williams, P. A. The atacamite family of minerals − a testbed for quantum spin liquids,. *Acta Crystallogr., Sect. B: Struct. Sci., Cryst. Eng. Mater.* **2018**, *74*, 519−526.
(37) Siidra, O. I.; Vladimirova, V. A.; Tsirlin, A. A.; Chukanov, N. V.; Ugolkov, V. L. $Cu_9O_2(VO_4)_4Cl_2$, the First Copper Oxychloride Vanadate: Mineralogically Inspired Synthesis and Magnetic Behavior,. *Inorg. Chem.* **2020**, *59*, 2136−2143.
(38) Siidra, O. I.; Zinyakhina, D. O.; Zadoya, A. I.; Krivovichev, S. V.; Turner, R. W. Synthesis and Modular Structural Architectures of Mineralogically Inspired Novel Complex Pb Oxyhalides,. *Inorg. Chem.* **2013**, *52*, 12799−12805.
(39) Usman, M.; Kocevski, V.; Smith, M. D.; Morrison, G.; Besmann, T.; Zur Loye, H. C. New Rubidium-Containing Mixed-Metal Hollandites,. *Cryst. Growth Des.* **2020**, *20*, 2398−2405.
(40) *APEX 3*, v2017.3; Bruker-AXS Inc.: Madison, WI, 2017.
(41) Sheldrick, G. M. A Short History of SHELX,. *Acta Crystallogr., Sect. A: Found. Crystallogr.* **2008**, *64*, 112−122.
(42) Morrison, G.; Zur Loye, H.-C. Simple correction for the sample shape and radial offset effects on SQUID magnetometers: Magnetic measurements on Ln_2O_3 (Ln = Gd, Dy, Er) standards,. *J. Solid State Chem.* **2015**, *221*, 334−337.
(43) Sanjeewa, L. D.; McMillen, C. D.; McGuire, M. A.; Kolis, J. W. Manganese Vanadate Chemistry in Hydrothermal BaF_2 Brines: $Ba_3Mn_2(V_2O_7)_2F_2$ and $Ba_7Mn_8O_2(VO_4)_2F_{23}$. *Inorg. Chem.* **2016**, *55*, 12512−12515.
(44) Pellizzeri, T. M. S.; McMillen, C. D.; Ivey, K.; Kolis, J. W. Crystal Structure and Preferential Site Occupancy in $Cs_6Mn(H_2O)_2(VO_3)_8$ and $Cs_5KMn(H_2O)_2(VO_3)_8$. *J. Chem. Crystallogr.* **2019**, *49*, 186−192.
(45) Sanjeewa, L. D.; Garlea, V. O.; McGuire, M. A.; McMillen, C. D.; Kolis, J. W. Magnetic ground state crossover in a series of glaserite systems with triangular magnetic lattices. *Inorg. Chem.* **2019**, *58*, 2813−2821.

(46) Smith Pellizzeri, T. M.; McGuire, M. A.; McMillen, C. D.; Wen, Y.; Chumanov, G.; Kolis, J. W. Two halide-containing cesium manganese vanadates: synthesis, characterization, and magnetic properties. *Dalton Trans.* **2018**, *47*, 2619−2627.
(47) Sanjeewa, L. D.; Garlea, V. O.; McGuire, M. A.; McMillen, C. D.; Cao, H.; Kolis, J. W. Structural and magnetic characterization of the one-dimensional S= 5/2 antiferromagnetic chain system SrMn (V O 4)(OH). *Phys. Rev. B: Condens. Matter Mater. Phys.* **2016**, *93*, 224407.
(48) Sanjeewa, L. D.; McGuire, M. A.; Garlea, V. O.; Hu, L.; Chumanov, G.; McMillen, C. D.; Kolis, J. W. Hydrothermal Synthesis and Characterization of Brackebuschite-type Transition Metal Vanadates: $Ba_2M(VO_4)_2(OH)$, M = V^{3+}, Mn^{3+} and Fe^{3+}, with Interesting Jahn-Teller and Spin-Liquid Behavior. *Inorg. Chem.* **2015**, *54*, 7014−7020.
(49) Smith Pellizzeri, T. M.; McMillen, C. D.; Wen, Y.; Chumanov, G.; Kolis, J. W. Iron Vanadates Synthesized from Hydrothermal Brines: $Rb_2FeV_6O_{16}$, $Cs_2FeV_6O_{16}$, and $SrFe_3V_{18}O_{38}$. *Eur. J. Inorg. Chem.* **2019**, *2019*, 4538−4545.
(50) Sanjeewa, L. D.; McGuire, M. A.; McMillen, C. D.; Garlea, V. O.; Kolis, J. W. Polar Materials with Isolated V^{4+} S = 1/2 Triangles: $NaSr_2V_3O_3(Ge_4O_{13})Cl$ and $KSr_2V_3O_3(Ge_4O_{13})Cl$,. *Chem. Mater.* **2017**, *29*, 1404−1412.
(51) Kimani, M. M.; McMillen, C. D.; Kolis, J. W. Hydrothermal Synthesis and Comparative Coordination Chemistry of New Rare-Earth V^{4+} Compounds,. *Inorg. Chem.* **2012**, *51*, 3588−3596.
(52) Schindler, M.; Hawthorne, F. C.; Baur, W. H. Crystal Chemical Aspects of Vanadium: Polyhedral Geometries, Characteristic Bond Valences, and Polymerization of (VO_n) Polyhedra,. *Chem. Mater.* **2000**, *12*, 1248−1259.
(53) Brese, N. E.; O'Keeffe, M. Bond-Valence Parameters for Solids,. *Acta Crystallogr., Sect. B: Struct. Sci.* **1991**, *47*, 192−197.
(54) Yakubovich, O. V.; Yakovleva, E. V.; Golovanov, A. N.; Volkov, A. S.; Volkova, O. S.; Zvereva, E. A.; Dimitrova, O. V.; Vasiliev, A. N. The First Vanadate−Carbonate, $K_2Mn_3(VO_4)_2(CO_3)$: Crystal Structure and Physical Properties,. *Inorg. Chem.* **2013**, *52*, 1538−1543.
(55) Smith Pellizzeri, T. M.; Sanjeewa, L. D.; Pellizzeri, S.; McMillen, C. D.; Garlea, V. O.; Ye, F.; Sefat, A. S.; Kolis, J. W. Single Crystal Neutron and Magnetic Measurements of $Rb_2Mn_3(VO_4)_2CO_3$ and $K_2Co_3(VO_4)_2CO_3$ with Mixed Honeycomb and Triangular Magnetic Lattices. *Dalton Trans.* **2020**, *49*, 4323−4335.
(56) Smith Pellizzeri, T. M.; Morrison, G.; McMillen, C. D.; zur Loye, H.-C.; Kolis, J. W. Sodium Transition Metal Vanadates from Hydrothermal Brines: Synthesis and Characterization of $NaMn_4(VO_4)_3$, $Na_2Mn_3(VO_4)_3$, and $Na_2Co_3(VO_4)_2(OH)_2$. *Eur. J. Inorg. Chem.* **2020**, *2020*, 3408−3415.
(57) Đordević, T.; Karanović, L. $Ba[Co_3(VO_4)_2(OH)_2]$ with a Regular Kagome Lattice,. *Acta Crystallogr., Sect. C: Cryst. Struct. Commun.* **2013**, *69*, 114−118.
(58) Sole, R.; Ruiz, X.; Gavalda, J.; Massons, J.; Sandiumenge, F.; Aguilo, M.; Diaz, F. Cobalt and tin substituted barium ferrites: the K and R phases,. *J. Appl. Phys.* **2000**, *87*, 1690−1692.
(59) Sandiumenge, F.; Gali, S.; Rodriguez-Clemente, R.; Batlle, X.; Obradors, X. $Ba_2Fe_{10}Sn_2CoO_{22}$: Growth, Crystal Structure (120 K), and Magnetic Properties,. *J. Solid State Chem.* **1991**, *92*, 213−218.
(60) Bonnet, P.; Payen, C.; Mutka, H.; Danot, M.; Fabritchnyi, P.; Stewart, J. R.; Mellergard, A.; Ritter, C. Spin correlations in the pyrochlore slab compounds $Ba_2Sn_2Ga_{10-7p}ZnCr_{7p}O_{22}$,. *J. Phys.: Condens. Matter* **2004**, *16*, S835−S842.
(61) Bono, D.; Mendels, P.; Collin, G.; Blanchard, N.; Baines, C.; Amato, A. A local study of dynamic and static magnetism in the Kagome bilayer compound $Ba_2Sn_2ZnCr_{6.8}Ga_{3.2}O_{22}$,. *J. Phys.: Condens. Matter* **2004**, *16*, S817−S822.
(62) Behera, P.; Ravi, S. Impedence spectroscopy and magnetic properties of Mg doped Y-type barium hexaferrite,. *J. Mater. Sci.: Mater. Electron.* **2018**, *29*, 20206−20215.
(63) Won, M. H.; Kim, C. S. Magnetic properties of Ni substituted Y-type barium ferrite,. *J. Appl. Phys.* **2014**, *115*, 17A509.
(64) Chang, Y.; Zhai, K.; Chai, Y.; Shang, D.; Sun, Y. Room-temperature magnetoelectric effects in multiferroic Y-type hexaferrites,. *J. Phys. D: Appl. Phys.* **2018**, *51*, 264002.
(65) Ferreira, T.; Morrison, G.; Chance, W. M.; Calder, S.; Smith, M. D.; Zur Loye, H.-C. $BaFe_4O_7$ and $K_{0.22}Ba_{0.89}Fe_4O_7$: Canted Antiferromagnetic Diferrites with Exceptionally High Magnetic Ordering Temperatures. *Chem. Mater.* **2017**, *29*, 2689−2693.

https://doi.org/10.1021/acs.chemmater.0c03852
Chem. Mater. 2021, 33, 2258−2266